Polymer Chemistry

PAPER

View Article Online
View Journal | View Issue

Cite this: *Polym. Chem.*, 2019, **10**, 3461

Supramolecular step-growth polymerization kinetics of pre-assembled triblock copolymer micelles†

Yingqing Lu,‡ Liang Gao,‡ Jiaping Lin,* Liquan Wang, Liangshun Zhang* and Chunhua Cai

The supramolecular polymerization of micelles and nanoparticles, drawing inspiration from the classic polymer science, provides an innovative concept to elucidate the organization of nanoscopic building units into one-dimensional hierarchical structures for wider applications in biotechnology and nanoscience. In contrast to the conventional molecular polymerization, the fundamental principles, especially the kinetics, of the supramolecular polymerization are rather less understood. Herein, capitalizing on the pre-assembled triblock copolymer micelles as prototypical systems, we propose a joint experimental-theoretical framework to probe into the mechanism and kinetics of the supramolecular polymerization. It is discovered that the self-assembly of micelles is induced by the structural defects where the core is partially exposed as a result of the imperfect coverage of the corona. The self-assembly of micelles reveals some similarities to molecular step-growth polymerization. A theoretical model of the supramolecular step-growth polymerization is proposed to complement the experimental results of defect-driven self-assembly kinetics, and reveals the essential distinction between the molecular and supramolecular polymerization kinetics. Furthermore, the kinetics and manner of self-assembly can be finely tuned by regulating the structural features of building units. These findings establish a quantitative framework for the supramolecular polymerization kinetics at the nanoscopic level that can aid in designing complex architectures and intrinsic properties of emerging materials.

Received 11th April 2019,
Accepted 22nd May 2019

DOI: 10.1039/c9py00539k

rsc.li/polymers

Introduction

Inspired by the sophisticated hierarchical materials in nature, researchers have pursued a diversity of strategies to the construction of nanomaterials with well-organized hierarchies.[1–3] Recently, step-wise self-assembly has emerged as an efficient strategy for developing multifarious hierarchical structures, among which the one-dimensional (1D) assemblies are of special interest due to a growing list of potential applications such as drug delivery vehicles, templates for the deposition of metal nanoparticles and catalysts.[4–8] The formed 1D hierarchical structure can be considered as a macroscopic counterpart of polymer chains, and the polymerization units are micelles or nanoparticles possessing specific sites for directional association.[9–12]

The deep understanding of the supramolecular polymerization mechanism of micelles and nanoparticles is of the essence for the rational design of 1D hierarchical structure. In order to achieve this perspective, researchers had their sight set on the conceptual analogy between molecular and supramolecular polymerizations. For example, Müller *et al.* probed into the formation of supracolloidal polymer chains from micellar subunits with tunable patches.[13,14] It was recently discovered by Ma *et al.* that the polymerization of those patchy micelles obeyed diffusion-controlled step-growth polymerization kinetics with a variable rate coefficient.[15,16] Winnik and Manners reported the 1D crystallization-driven self-assembly of polyferrocenylsilane block copolymers and demonstrated that the self-assembly followed the principles of living polymerization.[17,18] In spite of the advances, it is still an unattainable goal to establish the fundamental framework of the supramolecular polymerization. One of the roadblocks is the incomplete applicability of the kinetic model of conventional polymerization to some supramolecular polymerization

Shanghai Key Laboratory of Advanced Polymeric Materials, State Key Laboratory of Bioreactor Engineering, Key Laboratory for Ultrafine Materials of Ministry of Education, School of Materials Science and Engineering, East China University of Science and Technology, Shanghai 200237, China. E-mail: jlin@ecust.edu.cn, zhangls@ecust.edu.cn

†Electronic supplementary information (ESI) available: Experimental and simulation methods; control experiment; complementary characterization results; a theoretical model of the supramolecular polymerization of micellar subunits. See DOI: 10.1039/c9py00539k

‡These authors contributed equally.

systems as a result of the inherent distinction between the molecular monomer and nanoscale polymerization units.

For the "crew-cut" micelles, the 1D aggregation of the micelles is usually attributed to the interaction between the micelle coronas.[12,19,20] However, an alternative situation was recently discovered in which the aggregation is triggered by the hydrophobic interaction between the partially exposed core-forming chains.[21–24] This provides an inspiration for a versatile approach for the supramolecular polymerization by exploiting the micelles with structural defects on the core–corona interfaces. The defects of micelles exhibit the role of the reactive functional groups of molecular monomers in the step-growth polymerization. Nonetheless, the physical bonding between the defects is intrinsically different from the chemical reaction between the reactive groups. So far, little is known about this supramolecular polymerization strategy, including the range of application and the general rules. In particular, a kinetic model for the supramolecular polymerization has yet to be developed.

Herein, poly(γ-benzyl-L-glutamate)-*b*-poly(ethylene glycol)-*b*-poly(γ-benzyl-L-glutamate) (PBLG-*b*-PEG-*b*-PBLG) triblock copolymers were used as a model system to gain insight into the supramolecular polymerization driven by the defects. With the assistance of theoretical simulation, it was revealed that the rod-like micelles formed in the first-step assembly possess structural defects on the surfaces where the core is partially exposed as a result of the imperfect coverage of the corona. Induced by the structural defects, the rod-like micellar subunits were discovered to "polymerize" in a manner similar to the step-growth polymerization in the second-step assembly. However, the assembly of the micelles is different in kinetic rules from the step-growth polymerization since the structural defects are not exactly the same in size. We proposed a theoretical model for the micelle assembly, which provides a statistical explanation for the kinetics of the defect-driven supramolecular polymerization in experimental observations. In addition, the assembly manner and kinetics can be regulated by varying the location and size of the structural defects. The results deepen the understanding on the supramolecular polymerization mechanism and facilitate the controllable fabrication of 1D hierarchical materials.

Results and discussion

Supramolecular polymerization of PBLG-*b*-PEG-*b*-PBLG micellar subunits

The micellar subunits were first prepared and characterized. In the first-step assembly, the initial micellar subunits were self-assembled from the PBLG-*b*-PEG-*b*-PBLG triblock copolymers through the addition of a selective solvent (water) to the copolymer solution. After equilibration, the initial subunits were frozen by the rapid addition of a large amount of water and dialysis of the solution against water. The obtained aqueous solution was concentrated, preparing for the higher-level assembly. The detailed experiment procedures are provided in ESI, section 1.† Fig. 1a shows the TEM image of the micellar subunits self-assembled from the $PBLG_{252}$-*b*-PEG_{45}-*b*-$PBLG_{252}$ copolymer at 50 °C, where 252 and 45 denote, respectively, the repeating units of PBLG and PEG. The micelles show rod-like morphology with an approximate length and diameter of 220 and 65 nm, respectively. To examine the distribution of the polymer chains in the micelles, we stained the PEG chains with ruthenium tetroxide. As shown in the inset, the PEG corona around the micelles becomes relatively darker after staining. As can be seen, the ends of the micelles are not well

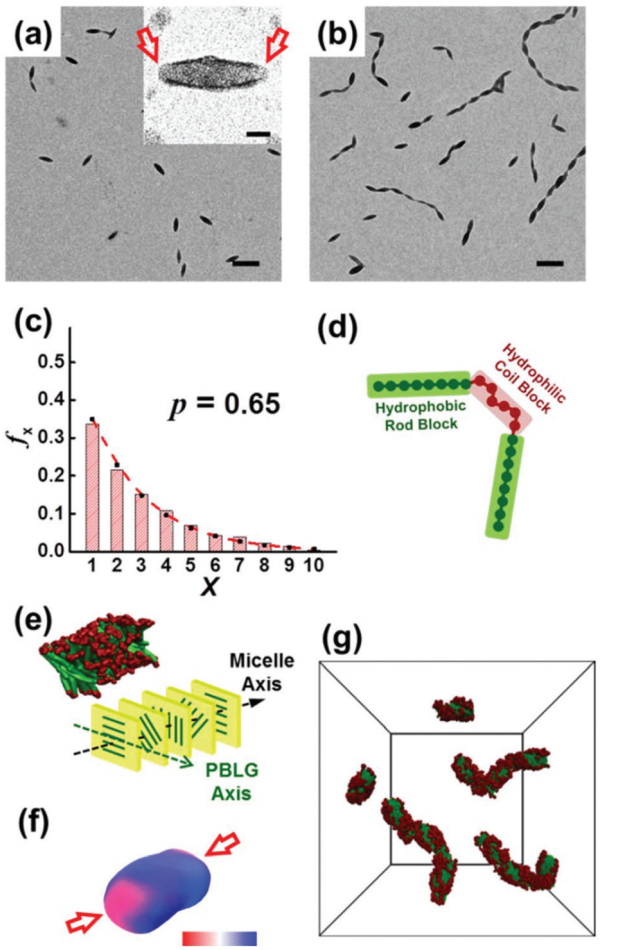

Fig. 1 Step-wise self-assembly of the $PBLG_{252}$-*b*-PEG_{45}-*b*-$PBLG_{252}$ copolymers into hierarchical nanowires. (a) Rod-like micelles self-assembled from the copolymers at 50 °C. Inset is the image of the micelle after staining the sample with ruthenium tetroxide. (b) TEM image of the nanowire aggregates formed from the rod-like micellar subunits after 24 day assembly. Scale bars: 400 nm for (a, b); 50 nm for the inset. (c) Number fraction (f_X) of the nanowires as a function of the degree of polymerization (X). The dashed line represents the theoretical number fraction of the nanowires ($f_X = (1 - p)p^{X-1}$). (d) Coarse-grained model of a rod-coil-rod triblock copolymer. (e) Simulation snapshots of the rod-like micelles ($\varepsilon_{RR} = 3.5\varepsilon$). The arrangement of PBLG chains in the micelle core is also illustrated. (f) Density distribution of the coil segment on the micelle core. The colours range from blue (high-density region) to red (low-density region). (g) Simulation snapshot of the end-to-end connected subunits from the pre-assembled rod-like micelles ($\varepsilon_{RR} = 5.0\varepsilon$).

covered by the corona (indicated by the red arrows). Here, we termed these regions where the corona cannot well cover the core the structural defects.

In the second-step assembly, DMF was added to the initial subunit solution. The addition of DMF leads to swelling of the micelle cores.[25] As a result, more core-forming chains are exposed at the structural defects, generating higher interfacial energy of the micelles. To reduce the unfavourable interfacial energy, the structural defects (which can be regarded as reactive points) could fuse with each other. After assembling for 24 days, the nanowire structures comprising of the end-to-end connected subunits were obtained (Fig. 1b). We found that the maximum length of the nanowires can be about 2 μm. The phenomenon indicates that those subunits act as nanoscale units for the 1D "supramolecular polymerization". The nanowire structure was also confirmed by cryo-TEM, which can rule out the possibility of drying artefacts (section 5 in the ESI†). Moreover, as shown in Fig. 1c, the number fraction f_X of the nanowires with degree of polymerization X can be fitted with the theoretical prediction of f_X in the step-growth polymerization of molecular monomers ($f_X = (1 - p)p^{X-1}$).[26] Here, X is defined as the number of micelles in a nanowire and p is the extent of polymerization, representing the fraction of polymerized micelles (see details in ESI, section 7). The result indicates that the growth follows a step-by-step manner, similar to the classical step-growth polymerization.

We then performed Brownian dynamics (BD) simulations to further examine the self-assembly behavior.[27–29] Corresponding to the PBLG-*b*-PEG-*b*-PBLG triblock copolymer, we constructed a coarse-grained model of rod–coil–rod copolymer, where each bead represents a cluster of atoms (Fig. 1d). The modeled triblock copolymer was denoted as $\mathbf{R_mC_nR_m}$, where **R**, **C**, and subscripts are the rod block (PBLG), the coil block (PEG), and the bead numbers of each block, respectively. The $\mathbf{R_{12}C_6R_{12}}$ copolymer was chosen based on the molecular structure of the copolymers in our experiments. The bead number of each block was set to match the relative length of the PBLG and PEG blocks (see details in section 13 of the ESI†). During the BD simulation, the amphiphilicity of the copolymers was realized by setting different interaction potentials. The interactions between **R** and **R** blocks (**R–R** interaction) were modelled with an attractive potential to describe the hydrophobicity of the PBLG blocks. The **C–C** and **R–C** interactions were modelled with a purely repulsive potential, corresponding to hydrophilic nature of the PEG blocks and the incompatibility between two blocks, respectively. In addition, the assembly of the copolymers was realized by setting different pairwise interaction parameters ε_{ij} (see details in ESI, section 13†). The strength of the solvophobic interaction was described by the interaction parameter ε_{RR} between **R** and **R** beads. When ε_{RR} was set as 3.5ε, corresponding to the condition of the first-step assembly (*i.e.* aggregation of the PBLG-*b*-PEG-*b*-PBLG copolymers), the $\mathbf{R_{12}C_6R_{12}}$ triblock copolymers can self-assemble into rod-like micelles. The rod blocks are orderly aligned in a twisted manner with the long axes perpendicular to the micelle long axis (Fig. 1e), which is similar to that reported in our previous study.[30] Such ordered packing of rod blocks causes the anisotropic distribution of the coil segments in the corona. To clearly characterize the distribution of the coil segments, we defined a parameter D_{coil} (the amount of **C** beads wrapping each **R** bead) to represent the density of the coil segments at different positions on the micelle core (see details in ESI, section 13†). The density distribution of the coil segments was indicated by colouring the micelle core according to the D_{coil} values (Fig. 1f). As can be seen, the coil segment density at the micelle ends is lower (as pointed out by the red arrows) than that at the body, suggesting that the ends of the micelle core can be to some extent exposed to the solvent.

In the second-step assembly, the micelles swell after the addition of DMF, causing more exposure of PBLG chains at the micelle ends to the solvent. As a result, the solvophobic interaction at the micelle ends increases. To simulate this situation, we increased the interaction parameter ε_{RR} to 5.0ε. In addition, considering that the molecular exchange between the micelles was hindered, the cores of the micelles were fixed (see details in ESI, section 13†). Under the new condition, the interfacial energy of the micelles increases. To reduce the unfavourable energy, the structural defects at the ends of the micelles fuse with each other, forming 1D assemblies (Fig. 1g). The details of the simulation are provided in sections 12 and 13 in ESI.† The simulation results well reproduced the two-step self-assembly behaviour observed in the experiments and indicated that the assembly of the triblock copolymer micelles is driven by the structural defects on the micelles.

As demonstrated above, in the rod-like micelles, the structural defects are located at the ends of the micelles, leading to the end-to-end connection of the micellar subunits. To further confirm the above mechanism, we carried out a control experiment by applying micelles possessing irregularly located structural defects as subunits for the second-step assembly. The micellar subunits for the control experiments are self-assembled from $PBLG_{167}$-*b*-PEG_{45}-*b*-$PBLG_{167}$. As shown in Fig. S4a,† the micellar subunits are nearly spherical and the structural defects are randomly located. The subunit structure was further revealed by the simulations. In these micelles, the rod blocks aggregate into the core in a radial manner and the coil blocks protrude outside to stabilize the spherical structure, leading to the randomly located structural defects on the micelles (Fig. S4c and e†). In the second-step assembly, these spherical micelles associate into agglomerates rather than in a 1D manner (Fig. S4b, d and f†). The disordered aggregation manner of these micelles is attributed to the irregular location of the structural defects. The above results manifest the mechanism of the step-wise self-assembly and reveal that the regular location of the structural defects is important for the occurrence of the controllable supramolecular polymerization.

The kinetics of the supramolecular polymerization was then studied. Fig. 2a–c and Fig. S7† show the aggregates self-assembled at different times. The length of the nanowires gradually increases and more subunits join in the nanowires with the progress of the polymerization (Fig. S10†). To observe the assembly process, we measured the apparent hydro-

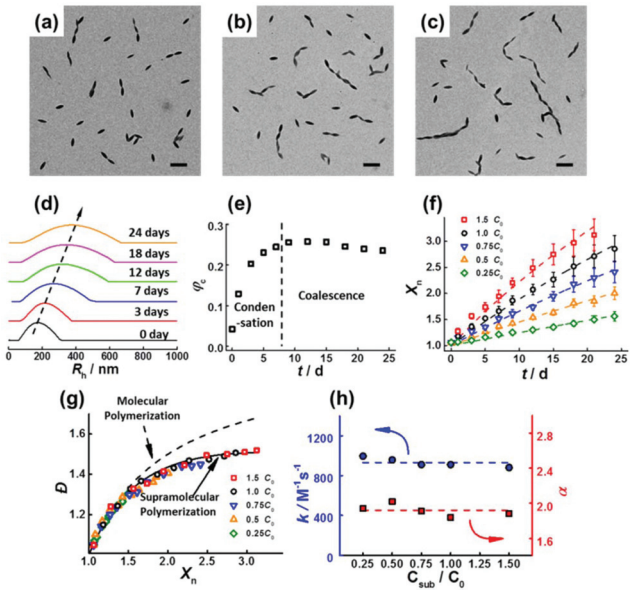

Fig. 2 Kinetics of the supramolecular polymerization. (a–c) Nanowire aggregates at different assembly times: (a) 1 day; (b) 12 days; and (c) 21 days. Scale bars: 400 nm. (d) Time evolution of $R_{h,app}$ distribution of the aggregates in solution. (e) Variation in the fraction of the supramolecular chains φ_c with time t. (f) Variation of the X_n *versus* t at various concentrations of the subunits. The dashed lines represent the fitting curve according to the supramolecular polymerization model. (g) Variation of the $Đ$ *versus* X_n. The solid line represents the fitting curve according to the supramolecular polymerization model. The dashed line represents the theoretical prediction of $Đ$ in the molecular step-growth polymerization ($Đ_{theory} = 2-1/X_n$). Here, the subunit concentration was adjusted through diluting the initial subunit solution into different volumes, and the value of C_{sub} at a polymer concentration of 0.2 g L^{-1} was designated as C_0. (h) Plots of the fitting α values and the assembly rate constants k with the variation of C_{sub}.

dynamic radius ($R_{h,app.}$) of the assemblies at different assembly times by dynamic light scattering (DLS) techniques (Fig. 2d). The peak maximum of $R_{h,app.}$ shifts toward a higher value and the $R_{h,app}$ distribution becomes broader with time, suggesting the progressive connection of the micelles. Since the DLS characterization was carried out *in situ*, the increase of $R_{h,app}$ is further evidence that the connection of the subunits occurs in solution instead of in the sample drying process.

The supramolecular chain growth process was further analysed through a quantitative approach. Fig. 2e displays the evolution of the fraction of the supramolecular chains φ_c with t. Details of the parameter definition and measurement are presented in ESI, section 7.† In the early stage of the assembly, φ_c increases rapidly resulting from the condensation of the subunits into the dimers and trimers. In the subsequent stage, φ_c reaches a plateau and gradually decreases, because the dimer and trimer structures are consumed when the dominant growth mechanism shifts to the oligomer coalescence. The evolution of φ_c suggests that the growth kinetics of the micellar subunits obeys the basic rule of the step-growth polymerization.[31]

To theoretically describe the kinetic process of the supramolecular step-growth polymerization in the experimental observations, we proposed a supramolecular polymerization model by adopting the mathematical method applied in the classic model for the step-growth polymerization.[31] Different from those in the conventional step-growth polymerization, the activities of the two reactive points of the subunit could be different since the two structural defects on the subunit are not exactly the same. This is evidenced by the different sizes of the structural defects (Fig. 1a) and the discrepant density distributions of the coil segments at the two micelle ends (Fig. 1f). The activity discrepancy of the reactive points can lead to the deviation of the supramolecular polymerization kinetics to that of the molecular polymerization. To describe the different activities of the two reactive points (denoted by **A** and **B**) of the micellar subunits, we introduced a parameter α in the model that is defined as the ratio of the activities between reactive points **A** and **B**. In this supramolecular polymerization, there are three different types of reaction, which are **A**-to-**A**, **A**-to-**B** and **B**-to-**B** reactions. The assembly rate constants of these three reactions are expressed as k, k/α and k/α^2, respectively. According to the model, we derived the following formulas of X_n and $Đ$ (see details in ESI, section 9†)

$$X_n = \frac{2(\alpha^2+1)kC_{sub}t + 2\alpha^2}{(\alpha-1)^2 kC_{sub}t + 2\alpha^2} \quad (1)$$

$$Đ = \frac{3\alpha^2 X_n + 2\alpha X_n - 2\alpha^2 + 3X_n - 2}{\alpha^2 X_n^2 - 2\alpha X_n^2 + X_n^2 + 4\alpha X_n} \quad (2)$$

Here, X_n is the number average degree of polymerization (representing the average length of the nanowires); $Đ$ is the dispersity (representing the length distribution of the nanowires); and C_{sub} is the subunit concentration that can be estimated through the light scattering technique (ESI, section 10†). Note that the equations are only suitable for the early stage of the polymerization, where p and X_n are in the following range: $0 < p < (\alpha+1)/2\alpha$ and $X_n < 2\alpha/(\alpha-1)$.

Fig. 2f and g display, respectively, the evolution of X_n with assembly time t and the variation of $Đ$ with X_n at different subunit concentrations. The lines in Fig. 2f and 2g show the fitted curves to the data based on eqn (1) and (2). As can be seen, the experimental data can be well fitted with the supramolecular polymerization model. In addition, the dashed line in Fig. 2g shows the theoretical prediction of $Đ$ in the step-growth polymerization of molecular monomers. The theoretical prediction values were obviously larger than the $Đ$ data, resulting from the unequal activity of the two reactive points of the subunits. The fitting values of α and k are shown in Fig. 2h. The best-fitting α values are around 1.92, and k at different subunit concentrations is almost constant with a value of around 930 M^{-1} s^{-1}. In the step-growth polymerization, the rate constant reflects the reaction activity of the monomers. The result shows that the assembly rate constant is considerably larger than the rate coefficient k of the step-growth polymerization of molecules (usually in the scope of

10^{-3}–10^{-5} M^{-1} s^{-1}). This is because the reaction between two functional groups in the conventional step-growth polymerization occurs only about once in every 10^{13} collisions.[31] However, in the supramolecular polymerization, the connection of two subunits requires many fewer collisions, depending on the size of the reactive points.[32] This can result in the higher polymerization rate of the supramolecular polymerization, which causes the higher k value. The fitting results indicate that the kinetics of supramolecular polymerization is distinct from the molecular polymerization.

Influence of micellar subunit structure on supramolecular polymerization

In the polymerization of molecular monomers, it is a universal principle that the polymerization process is significantly affected by the monomer structure. Inspired by this fact, we assume that the supramolecular polymerization behaviour can also be influenced by the micellar subunit structure. To verify this assumption, we examined the influence of the micellar subunit structure on the supramolecular polymerization. Here, the micelles with various structures can be formed under different self-assembly temperatures.[33]

Fig. 3a and b show the TEM images of the $PBLG_{252}$-*b*-PEG_{45}-*b*-$PBLG_{252}$ micelles prepared at 30 and 10 °C, respectively. For convenience, the micellar subunits prepared at different temperatures were named as subunit I (50 °C), subunit II (30 °C) and subunit III (10 °C). First, the structures of the micellar subunits were examined. The subunits II and III are ellipsoid-like, and the diameter of the micelles increases with the decreasing micellization temperature. Additionally, different from that of the subunit I, the structural defects of the subunits II and III can be at both the side face and ends of the micelles (shown in the insets).

To gain more information about the subunit structure, we performed simulation of the formation of the subunits II and III. The decreased temperature leads to weaker interaction between the PBLG segments.[33] To simulate this variation of self-assembly condition, we decreased the interaction strength ε_{RR}. As ε_{RR} is decreased to 3.2ε, ellipsoid-like micelles are obtained, corresponding to the subunit II (Fig. 3c). The rod blocks are perpendicular to the long axis of the micelles. As revealed by the density distribution of the coil segments (Fig. 3d), the exposed area of the core is mainly located at the ends (pointed out by the red arrow), while the side of the core can also have exposed area due to the increased diameter of the ellipsoid-like micelles than that of the rod-like micelles. With further decreasing the interaction parameter to 2.6ε, ellipsoid-like micelles with larger diameters can be observed, which correspond to the subunit III (Fig. 3e). In these micelles, the rod blocks aggregate to form the micelle core in a double-deck radial manner. The exposed area of the solvophobic core can be away from the ends of the micelle (shown by the red arrow in Fig. 3f). In addition, the exposure area of the core is smaller in this micelle than that in the micelle obtained at 3.2ε. These simulation results accord with the TEM characterization in the experiments.

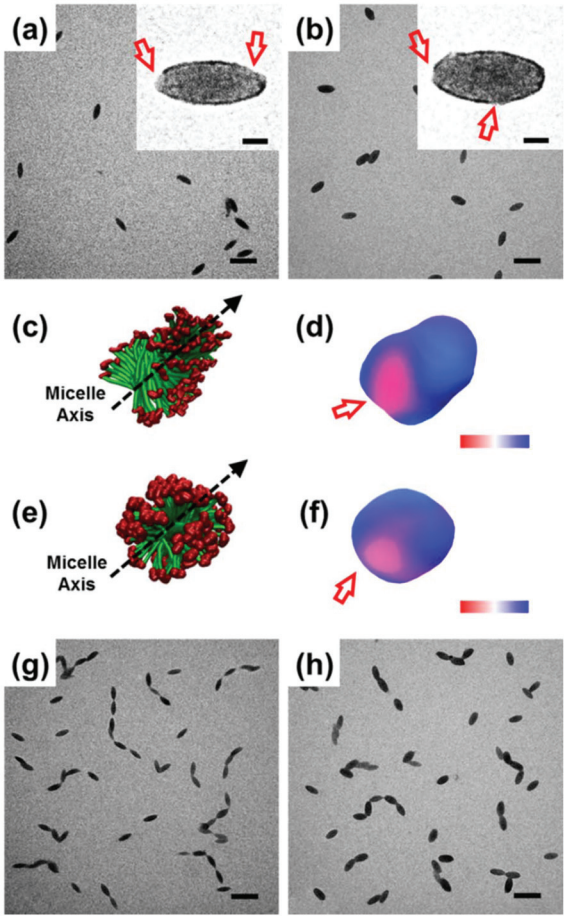

Fig. 3 Self-assembly of the copolymer micellar subunits with different structures. (a, b) TEM images of the ellipsoids-like subunits (a) II and (b) III. Insets are the images of the micelles after staining the samples with ruthenium tetroxide. (c, d) The (c) simulation snapshot of the ellipsoidal micelles and the (d) corresponding presentation of the density distributions of the coil segments at $\varepsilon_{RR} = 3.2\varepsilon$. (e, f) The (e) simulation snapshot of the ellipsoidal micelles and the (f) corresponding presentation of the density distributions of the coil segments at $\varepsilon_{RR} = 2.6\varepsilon$. The colours in d and f range from blue (high-density region) to red (low-density region). (g, h) TEM images of aggregates formed from the subunits (g) II and (h) III after assembling for 24 days. Scale bars: 400 nm; 50 nm for the insets of (a, b).

The above results reveal that the location and size of the structural defects on the micelles are changed when the micelle structure varies with decreasing micellization temperature. The connecting behaviours of these micelles with different structures were then examined. Fig. 3g and h are the TEM images of the aggregates formed from the subunits II and III after 24 days of assembly, respectively. The connected structures were also confirmed by cryo-TEM, which rules out the effect of the drying process (Fig. S5†). The extents of polymerization p at 24 days are 0.56 for the subunit II and 0.41 for the subunit III (Fig. S11 and S12†), which are lower than that of the subunit I (Fig. 1c). The results suggest that the fraction of subunits joining in the nanowire decreases from the subunit I to the subunit III.

Moreover, the connecting manner of the subunits is to some degree changed. For these micellar subunits, there are mainly three connecting manners: end-to-end, end-to-side and side-to-side. Fig. 4 shows the typical TEM images of these three connecting manners and the number fractions of the connecting manners for different subunits. A majority (>80%) of the subunit I are connected in an end-to-end manner. However, for the subunit II, the number fraction of the end-to-side and side-to-side connecting manners slightly increases and this increase is more obvious for the subunit III. It should be mentioned that the subunits are occasionally connected with more than two subunits, leading to a very small fraction of branching structures or disorderly aggregated structures (Fig. S6†). Such phenomenon occurs because the subunit possesses three reactive points or one reactive point on the subunit bonds with two other reactive points.

In addition to the connecting manner, we also investigated the influence of the subunit structure on assembly kinetics using the supramolecular polymerization model. Fig. 5a–d shows the variation of X_n *vs.* t and $Đ$ *vs.* X_n of the subunits II and III. The experimental data can also be fitted with the proposed model of supramolecular polymerization. In addition, $Đ$ was smaller than the theoretical prediction in the classical step-growth polymerization (as indicated by the dashed line in Fig. 5c and d). It should be noted that all the subunits are hypothesized to possess two reactive points in the data analysis, since the fraction of subunits with more than two reactive points is low. The obtained values of α and the assembly rate constants k are plotted in Fig. 5e and f, respectively. The values of α and k are not influenced by the subunit concentration, which is similar to that of the subunit I. The average fitting values of α are 2.10 for the subunit II and 2.50 for the subunit III, while α is 1.92 for the subunit I (Fig. 2h). The change of the α value indicates that the difference in the activities between the reactive points becomes larger from the subunit I to III. In addition, the average values of k are 550 M^{-1} s^{-1} for the subunit III and 800 M^{-1} s^{-1} for the subunit II, respectively,

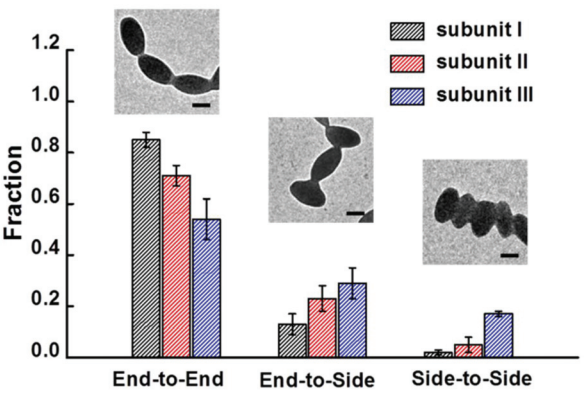

Fig. 4 The number fractions of the different connecting manners for the three types of micelles. Insets are the typical images of the end-to-end, end-to-side and side-to-side connecting manners. Scale bars: 100 nm.

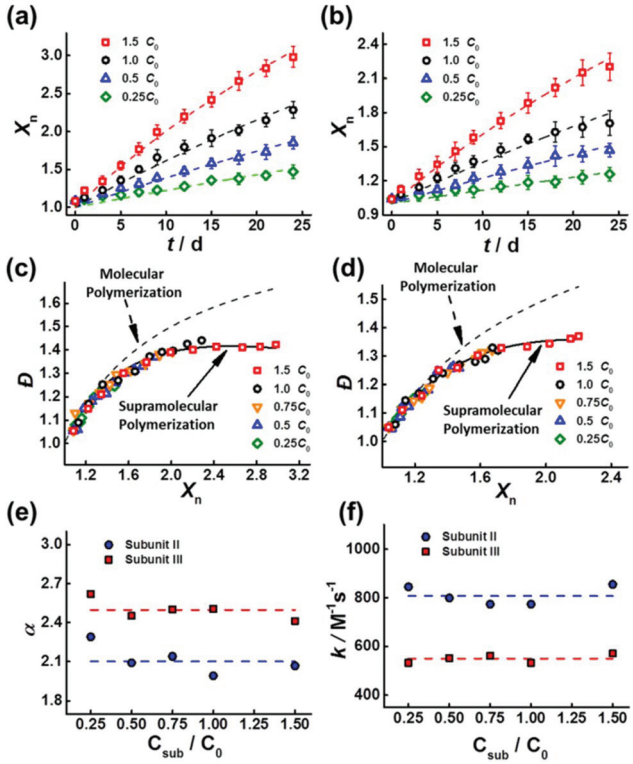

Fig. 5 Polymerization kinetics of the micellar subunits with different structures. (a, b) Variation of the X_n *versus* the assembly time t, at various concentrations of the subunits (a) II and (b) III. The dashed lines represent the fitting curve according to the supramolecular polymerization model. (c, d) Variation of the $Đ$ *versus* X_n of the subunits (c) II and (d) III. The solid line represents the fitting curve according to the supramolecular polymerization model. The dashed line represents the theoretical prediction of $Đ$ in the molecular step-growth polymerization ($Đ_{theory}$ = $2-1/X_n$). (e, f) Plots of the fitting (e) α and (f) k values of the subunits II and III at different C_{sub}.

while the assembly rate constant of the subunit I is 930 M^{-1} s^{-1} (Fig. 2h). The gradual increase of the assembly rate from the subunit III to I is associated with the higher activity of the reactive points resulting from the increased size of the structural defects. The above results suggest that the assembly manner and rate of the micellar subunits can be modulated by the location and size of the structural defects.

Additionally, we examined the influence of the copolymer composition on the supramolecular polymerization (see section 11 of the ESI†). When the repeating units of PBLG vary from 206 to 167 and 108 (the repeating units of PEG are 45), the morphology of the micellar subunits changes from rod to sphere. In the corresponding second assembly step, the aggregation of the subunits is more irregular and the number of one-dimensional structures decreases with decreasing PBLG length. The results indicate that the supramolecular polymerization is more likely to occur with the longer length of the PBLG blocks. This is because the change of the copolymer composition can also result in the variation of the location and size of the structure defects, which affects the supramolecular polymerization of the micellar subunits.

In the present work, we studied the defect-driven supramolecular polymerization of the triblock copolymer micelles. The defect-driven supramolecular polymerization is a 1D assembly process triggered by the structural defects on the micellar subunits where the corona cannot well cover the core. As revealed by the results, we found out some common features of the defect-driven supramolecular polymerization. (1) The supramolecular polymerization is a versatile assembly strategy for the micellar subunits possessing structural defects. Accumulation of the experimental and simulation results demonstrates that the micellar subunits can assemble into hierarchical structures under appropriate conditions as long as there are structural defects on the micelles. (2) The structural defects are not exactly the same, which leads to the different activities of the reactive points and thus the complicated polymerization kinetics. Given this fact, we proposed a kinetic model of the defect-driven supramolecular polymerization. (3) The location and size of the structural defects are important factors influencing the defect-driven supramolecular polymerization.

It should be noted that the controllable supramolecular polymerization cannot occur when the structural defects on the micellar subunits are irregularly located. This is evidenced by our control experiments mentioned above (see details in section 4 of ESI†). Moreover, in the literature, it is widely reported that micelles with isotropic or polydisperse structures aggregate into agglomerates and the assembly is disordered.[34,35] This is because the micelles possess structural defects which can serve as binding sites for the assembly, but the structural defects are randomly distributed. As long as the location and size of the structural defects can be delicately designed, the micelles can aggregate into a well-organized 1D structure. The knowledge obtained from the present work can provide useful information for manipulating such assembly systems and realizing the controllable supramolecular polymerization.

In addition, it is worth mentioning that the supramolecular polymerization model in the work can further be improved. In the present model, it is assumed that all the micellar subunits are homologous, possessing two reactive points with a certain activity ratio. However, the structure of the micellar subunits can be more complicated in reality. For example, the reactive points can be dispersive with a continuum of sizes. Taking this into consideration, the values of the activity ratio of the reactive points α and the assembly rate constant k should be variable within a certain range. The refinement of the model is essential for the supramolecular polymerization to go beyond the features of the molecular polymerization, which may be the focus of future related works.

Conclusions

In this work, we reported the 1D assembly of pre-assembled PBLG-*b*-PEG-*b*-PBLG micelles and proposed the general concept of the defect-driven supramolecular polymerization of the micellar subunits with the assistance of theoretical simulation. The results implied the versatility of the defect-driven supramolecular polymerization. We proposed a quantitative kinetic model for the analysis and prediction of the defect-driven supramolecular polymerization. Moreover, when the size and location of the structural defects are changed, the assembly kinetics as well as the assembly manners of the subunits is varied accordingly. The above knowledge obtained from the work can deepen our understanding of the supramolecular polymerization of micellar subunits. In addition, the results can offer guidance to the design of micellar subunits for constructing well-ordered supramolecular materials.

Experimental section

Polymer synthesis

PBLG-*b*-PEG-*b*-PBLG was synthesized through the ring-opening polymerization of γ-benzyl-L-glutamate-*N*-carboxyanhydride (BLG-NCA) initiated by α,ω-diamino-poly(ethylene glycol) (NH_2-PEG-NH_2) (M_w = 2000) with 1,4-dioxane as the solvent.[36,37] After sufficient reaction, the product was precipitated in anhydrous methanol. The detailed information is shown in section 1 of ESI.†

Step-wise self-assembly

In the first-step assembly, initial micellar subunits were prepared. In a typical experiment, PBLG-*b*-PEG-*b*-PBLG copolymers were dissolved in THF/DMF (1/1, v/v) mixture solvents (polymer concentration of initial solution was 0.25 g L^{-1}). To prepare the initial micelle solution, deionized water was added dropwise to the PBLG-*b*-PEG-*b*-PBLG initial solution with vigorous stirring, reaching a water content of 16.7 vol%. By adjusting temperature in the above processes, the structure of the subunits could be adjusted. After equilibration, the initial subunits were frozen *via* rapid addition of plenty of water and dialysis against water. The obtained aqueous solution of the initial subunits was concentrated with a rotary evaporator to a final concentration of 0.6 g L^{-1}. For the studies of the effect of the subunit concentration on the higher-level assembly, the concentrated aqueous subunit solution was diluted into different volumes *via* addition of water.

In the second-step assembly, DMF was added to the solution of subunits (DMF content was 50 vol%). The subunits were thus activated and the assembly began. To characterize the aggregate morphologies at different experimental intervals, the morphologies were frozen by rapid addition of plenty of water and dialysis against water before observation. The second-step assembly was conducted at the constant temperature of 30 °C.

Simulation methods

BD is a coarse-grained mesoscopic simulation method.[27,29,38] In the simulation, each bead represents a cluster of atoms and is connected by the bond stretching potential. Due to the rigid α-helix conformation of PBLG, the PBLG-*b*-PEG-*b*-PBLG tri-

block copolymer can be regarded as a rod–coil–rod triblock copolymer model. The rigidity of the rod blocks and the pairwise interaction are described by the angle bend potential and the Lennard-Jones potential, respectively. The time evolution of the beads obeys the Langevin equation. The simulations were conducted in a cubic box of 100 × 100 × 100 with periodic boundary conditions, and an NVT ensemble was adopted. Details regarding the simulations can be found in sections 12 and 13 of ESI.†

Conflicts of interest

There are no conflicts to declare.

Acknowledgements

This work was supported by the National Natural Science Foundation of China (51833003, 51621002, 21474029, 51573049). Support from projects of the Shanghai municipality (16520721900) is also appreciated.

Notes and references

1 R. Shrestha, M. Elsabahy, H. Luehmann, S. Samarajeewa, S. Florez-Malaver, N. S. Lee, M. J. Welch, Y. Liu and K. L. Wooley, *J. Am. Chem. Soc.*, 2012, **134**, 17362–17365.
2 X.-S. Hou, G.-L. Zhu, L.-J. Ren, Z.-H. Huang, R.-B. Zhang, G. Ungar, L.-T. Yan and W. Wang, *J. Am. Chem. Soc.*, 2018, **140**, 1805–1811.
3 W. M. Aumiller, M. Uchida, D. W. Biner, H. M. Miettinen, B. Lee and T. Douglas, *Chem. Mater.*, 2018, **30**, 2262–2273.
4 A. Wang, J. Huang and Y. Yan, *Soft Matter*, 2014, **10**, 3362–3373.
5 A. H. Gröschel and A. H. E. Müller, *Nanoscale*, 2015, **7**, 11841–11876.
6 D. Xia, Z. Ku, D. Li and S. R. J. Brueck, *Chem. Mater.*, 2008, **20**, 1847–1854.
7 Z. Zhang, C. Zhou, H. Dong and D. Chen, *Angew. Chem., Int. Ed.*, 2016, **128**, 6290–6294.
8 X. Li, B. Jin, Y. Gao, D. W. Hayward, M. A. Winnik, Y. Luo and I. Manners, *Angew. Chem., Int. Ed.*, 2016, **55**, 11392–11396.
9 J. Zhu, S. Zhang, F. Zhang, K. L. Wooley and D. J. Pochan, *Adv. Funct. Mater.*, 2013, **23**, 1767–1773.
10 X. Yan, G. Liu and Z. Li, *J. Am. Chem. Soc.*, 2004, **126**, 10059–10066.
11 H. Jin, Y. Zhou, W. Huang and D. Yan, *Langmuir*, 2010, **26**, 14512–14519.
12 J.-H. Kim, W. J. Kwon and B.-H. Sohn, *Chem. Commun.*, 2015, **51**, 3324–3327.
13 A. H. Gröschel, F. H. Schacher, H. Schmalz, O. V. Borisov, E. B. Zhulina, A. Walther and A. H. E. Müller, *Nat. Commun.*, 2012, **3**, 710–720.
14 A. H. Gröschel, A. Walther, T. I. Lobling, F. H. Schacher, H. Schmalz and A. H. E. Müller, *Nature*, 2013, **503**, 247–251.
15 X. Ma, Y. Zhou, L. Zhang, J. Lin and X. Tian, *Nanoscale*, 2018, **10**, 16873–16880.
16 X. Ma, M. Gu, L. Zhang, J. Lin and X. Tian, *ACS Nano*, 2019, **13**, 1968–1976.
17 J. B. Gilroy, T. Gädt, G. R. Whittell, L. Chabanne, J. M. Mitchels, R. M. Richardson, M. A. Winnik and I. Manners, *Nat. Chem.*, 2010, **2**, 566–570.
18 H. Qiu, Z. M. Hudson, M. A. Winnik and I. Manners, *Science*, 2015, **347**, 1329–1332.
19 X.-X. Xia, Q. Xu, X. Hu, G. Qin and D. L. Kaplan, *Biomacromolecules*, 2011, **12**, 3844–3850.
20 L. Ma, H. Geng, J. Song, J. Li, G. Chen and Q. Li, *J. Phys. Chem. B*, 2011, **115**, 10586–10591.
21 Z. Li, J. Ma, N. S. Lee and K. L. Wooley, *J. Am. Chem. Soc.*, 2011, **133**, 1228–1231.
22 Z. Zhuang, T. Jiang, J. Lin, L. Gao, C. Yang, L. Wang and C. Cai, *Angew. Chem., Int. Ed.*, 2016, **55**, 12522–12527.
23 H. Tan, Z. Wang, J. Li, Z. Pan, M. Ding and Q. Fu, *ACS Macro Lett.*, 2013, **2**, 146–151.
24 C. Yang, X. Ma, J. Lin, L. Wang, Y. Lu, L. Zhang, C. Cai and L. Gao, *Macromol. Rapid Commun.*, 2018, **39**, 1700701.
25 R. A. I. Orwoll, *Polymer Handbook*, Wiley, New York, 3rd edn., 1989.
26 G. Odian, *Principles of Polymerization*, Wiley, New York, 4th edn., 2004.
27 G. S. Grest and K. Kremer, *Phys. Rev. A*, 1986, **33**, 3628.
28 S. Lin, N. Numasawa, T. Nose and J. Lin, *Macromolecules*, 2007, **40**, 1684–1692.
29 Q. Zhang, J. Lin, L. Wang and Z. Xu, *Prog. Polym. Sci.*, 2017, **75**, 1–30.
30 W. Ding, S. Lin, J. Lin and L. Zhang, *J. Phys. Chem. B*, 2008, **112**, 776–783.
31 P. J. Flory, *Principles of Polymer Chemistry*, Cornell University Press: Ithaca, New York, 1953.
32 Y. Wang, Y. Wang, D. R. Breed, V. N. Manoharan, L. Feng, A. D. Hollingsworth, M. Weck and D. J. Pine, *Nature*, 2012, **491**, 51–55.
33 C. Cai, Y. Li, J. Lin, L. Wang, S. Lin, X.-S. Wang and T. Jiang, *Angew. Chem., Int. Ed.*, 2013, **52**, 7732–7736.
34 Y. Tu, Z. Ji, X. Yang, X. Wan and Q. F. Zhou, *Macromol. Rapid Commun.*, 2014, **35**, 1795–1800.
35 R. Huang, D. Chen and M. Jiang, *J. Mater. Chem.*, 2010, **20**, 9988–9994.
36 P. Doty, J. H. Bradbury and A. M. Holtzer, *J. Am. Chem. Soc.*, 1956, **78**, 947–954.
37 T. J. Deming, *Adv. Polym. Sci.*, 2006, **202**, 1–18.
38 L. Gao, J. Lin, L. Zhang and L. Wang, *Nano Lett.*, 2019, **19**, 2032–2036.

